Electrochemical performance comparison of MWCNTs/Ni $(OH)_2$ composite materials by two preparation routes

M. G Ortiz[1,2] · E. B Castro[1] · S. G. Real[1]

Abstract Carbon materials are used to improve the nickel hydroxide electrode capacity in rechargeable alkaline batteries. Herein, we present the preparation of multiwall carbon nanotubes/nickel hydroxide composites (MWCNTs/Ni $(OH)_2$) by two different routes. The first method consists of the direct incorporation of MWCNTs in the active material, and the second is based on the hydrothermal synthesis of β-nickel hydroxide, where MWCNTs are added to the precursor solutions. The electrochemical properties of the prepared positive electrodes containing MWCNTs/Ni $(OH)_2$ composites are studied. Electrochemical results indicate that the active material with MWCNTs incorporated before the hydrothermal synthesis is capable of delivering a higher discharge capacity and exhibits a better reversibility than those composites prepared with MWCNTs after the hydrothermal route.

Keywords Nickel hydroxide · Carbon nanotubes · Positive electrode · Ni-MH batteries

Castro E.B. passed away on February 18th, 2013.

✉ M. G Ortiz
mortiz@inifta.unlp.edu.ar

✉ S. G. Real
sreal@inifta.unlp.edu.ar

[1] Instituto de Investigaciones Fisicoquímicas Teóricas y Aplicadas (INIFTA), Facultad de Ciencias Exactas, Universidad Nacional de La Plata, Suc. 4, C.C.16, 1900 La Plata, Argentina

[2] Centro de Investigación, Desarrollo en Ciencia y Tecnología de los Materiales (CITEMA), Facultad Regional La Plata, Universidad Tecnológica Nacional, Calle 60 y 124, Berisso, Argentina

Introduction

Numerous studies have been previously done to improve the performance of cathode materials for alkaline secondary batteries, based on the incorporation of additives in the Ni $(OH)_2$ active material, such as Co, Cd, Ca, C, Zn, Al, and Ba [1–9] elements. Furthermore, graphite and acetylene black have been employed to enhance the electronic conductivity and utilization of the active material in nickel hydroxide electrodes [6, 7, 10]. Among carbon compounds, carbon nanotubes (CNTs) have excellent mechanical properties, which are high elastic modulus (1.8 TPa) [11] and flexural strength (14.2 GPa) [12], good toughness [13], and high conductivity [14–16].

Early studies showed that a continuous expansion and contraction of the nickel hydroxide electrode occurs during the battery charge and discharge processes. Consequently, the active material loses its mechanical strength, becomes detached from the substrate, and gives rise to higher internal resistance and lower capacity values. Unlike other carbonaceous materials such as graphite, the specific volume of the CNT monomer is much smaller and its specific surface is much greater. Thus, the continuous conductive CNT mesh generated inside these electrodes would provide the benefit of increasing the stability of the phase β-Ni $(OH)_2$ by improving its mechanical resistance during charge and discharge processes. The high expansion coefficient values along the axial direction of the CNT could increase the elasticity of cathodes and prevent the release of the active material [17]. Furthermore, the nanometric size of these materials would lead to chemical stability improvement and a high surface area.

CNTs are promising materials to be used in different storage and energy conversion systems, such as supercapacitors [18–21], hydrogen storage materials for batteries (i.e., Ni-MH), and fuel cells [22, 23], as well as anode materials in lithium batteries [24, 25]. The effects of CNTs as additive on

the properties of nickel hydroxide electrodes in AA Ni-MH batteries were first investigated by Lev et al. [26]. They found that the addition of CNTs may improve battery performance at high discharge rate. Other researchers, such as Song et al. [17], studied the addition of CNTs to nickel hydroxide powder for rechargeable batteries and came to the conclusion that the utilization of the active material as well as its specific discharge capacity could be increased. It should be noted here that previous impedance results [17] were interpreted with simplified equivalent circuits that are not able to account for the physicochemical and structural parameters that govern the electrochemical behavior of the system. Taking into consideration all these facts, in this work, CNTs are added to nickel hydroxide active materials, employing different synthesis routes, in order to investigate the main parameters that control their electrochemical performance.

Experiment

β-Ni $(OH)_2$ was obtained as final product when Ni (SO_4) and NaOH aqueous solutions were mixed and placed in Teflon-lined autoclave at 180 °C for 24 h, using the typical process of hydrothermal synthesis described in our previous publication [27].

Commercial MWCNTs (2 wt%, Aldrich, purified by immersion in a concentrated nitric acid) were incorporated as additive in β-Ni $(OH)_2$ by two different methods:

- Physical mixture of the β-Ni $(OH)_2$ active material previously obtained by hydrothermal synthesis (MWCNTsNi-PhM)
- Added to precursor solutions before hydrothermal synthesis, as previously described [28] (MWCNTsNi-PS).

The prepared composites were characterized by X-ray diffraction (XRD; PW-1730 Philips X-ray diffractometer with Cu-Kα radiation) and transmission electron microscopy (TEM; Jeol JEM 1200EX II model).

The electrochemical measurements were carried out using a classical three-compartment glass cell containing 7 M KOH solutions at 30 °C.

The working electrodes were prepared by mixing the active material (commercial Ni $(OH)_2$, MWCNTsNi-PhM, or MWCNTsNi-PS) with teflonized carbon black (Vulcan XC-72, with 30 wt% PTFE) as the binder, in a weight ratio of 65:35. The obtained mix was pasted onto nickel foam current collectors of 0.4-cm^2 area and 0.075 cm thick. These prepared working electrodes are named, which are E-Ni-com, E-MWCNTsNi-PhM, and E-MWCNTsNi-PS.

A nickel mesh of large specific area and Hg/HgO_{ss} were used as counter and reference electrodes, respectively. All potentials in this text are referred to the Hg/HgO_{ss} electrode.

Cyclic voltammetry (CV) curves were measured using Gamry Reference 3000 potentiostat at a scan rate of 1 mV s^{-1}, between 0.05- and 0.55-V potential limits. The charge and discharge measurements were carried out employing Arbin Instruments model BT2000 potentiostat, at different current densities within a voltage range of 0.2–0.55 V. The electrochemical impedance spectroscopy (EIS) experiments were performed using a frequency response analyzer Solartron 1250 coupled to an EG&G potentiostat model PAR 273. Before each EIS experiment, the working electrodes were activated by charging at a current corresponding to C/2 and discharging at the same current, until a constant capacity was reached. After this procedure, the electrodes were discharged up to 50% state of discharge (SOD), and the EIS measurements were performed potentiostatically at the open circuit potential.

For the sake of comparison, the EIS experiments were conducted in the frequency range between 65 KHz and 1.99 mHz, with a perturbation signal amplitude of 5 mV, at constant SOD.

The surface morphology of electrodes was examined by scanning electron microscopy (SEM) employing a Philips SEM, model 505, with an image digitizer system (Soft Imaging ADDA II).

Results and discussion

The XRD patterns of samples are presented in Fig. 1, and all diffraction peaks can be readily indexed to the hexagonal β-Ni $(OH)_2$ according to the JCPDS file no. 14–0117. Figure 1c shows that the MWCNTsNi-PS composite exhibits a diffraction peak at $2\theta = 24°$ corresponding to the (002) plane of MWCNTs. Figure 1b, c shows that the difference in the relative intensity of diffraction peaks can be related to their differences in microstructure and morphology.

The morphologies of the studied materials are shown in Fig. 2 (TEM images). It can be clearly seen that commercial nickel hydroxide samples (Fig. 2a) exhibit spherical particle agglomerations. A remarkably different morphology was obtained with nickel hydroxide materials synthesized by hydrothermal route. It this case, a nanosized ribbon appearance was observed (Fig. 2b). Similarly, ribbon structures with larger widths are obtained for MWCNTsNi-PS samples (Fig. 2c). It is apparent that the incorporation of MWCNTs along with precursor solutions influences ribbon widths. These facts can be explained taking into consideration that their own shape could provide a base structure that favors the nucleation and growth processes of nickel hydroxide. TEM images with higher magnification (Fig. 2c) allow seeing an internal structure of thin curve threads that would correspond to the MWCNT base structures [17] in good agreements with publish literature.

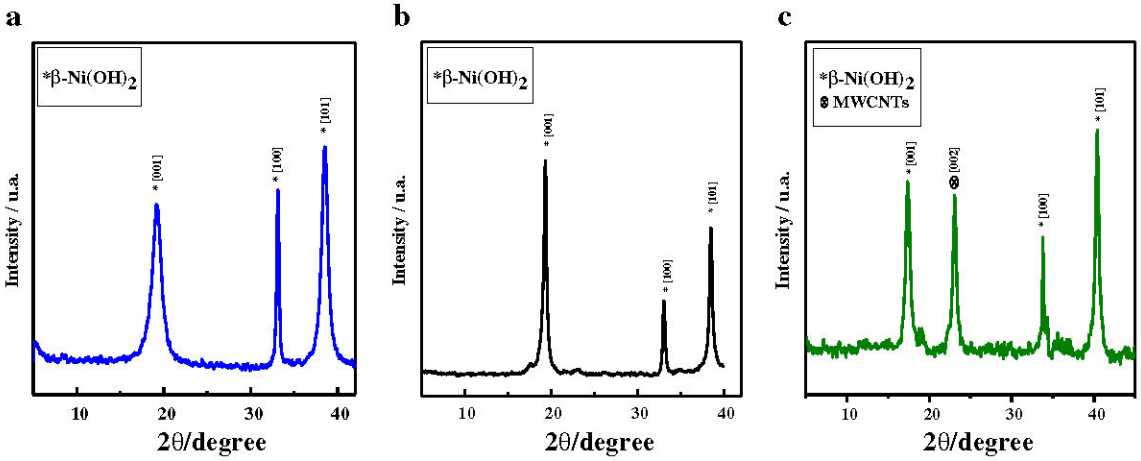

Fig. 1 XRD spectra of **a** Ni-com, **b** MWCNTsNi-PhM, and **c** MWCNTsNi-PS

Figures 3, 4, and 5 show the SEM images of working electrodes after stabilizing the galvanostatic charge-discharge cycling profile. These results indicate that the surface topography has a porous net-like structure that may facilitate electrolyte soaking into particles, as well as the insertion and de-insertion of protons during the charge-discharge process. However, for MWCNTsNi-PS samples, more porous surface structures can be observed (Figs. 3, 4, and 5).

Figure 6 shows the stabilized CV curves of the studied samples after 7 cycles. The seventh cycle was used for comparison because all the studied systems presented not modifications of their CV profiles after that cycle. The

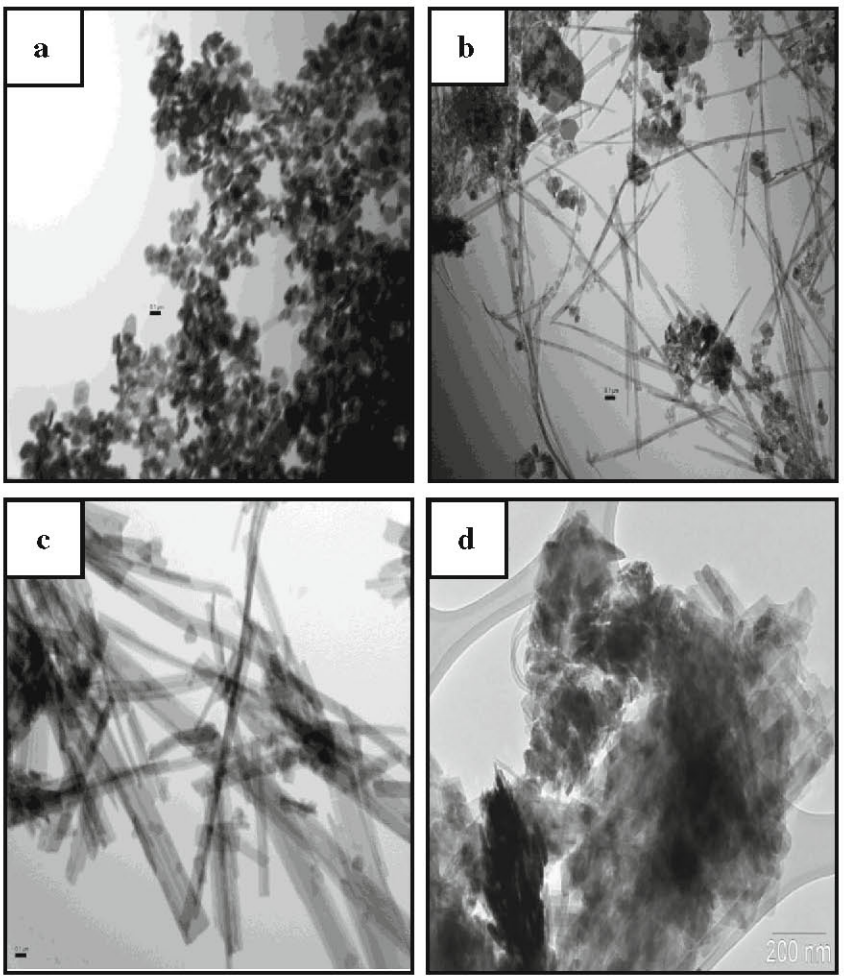

Fig. 2 TEM images of **a** Ni-com, **b** nickel hydroxide by hydrothermal synthesis, and **c**, **d** MWCNTsNi-PS

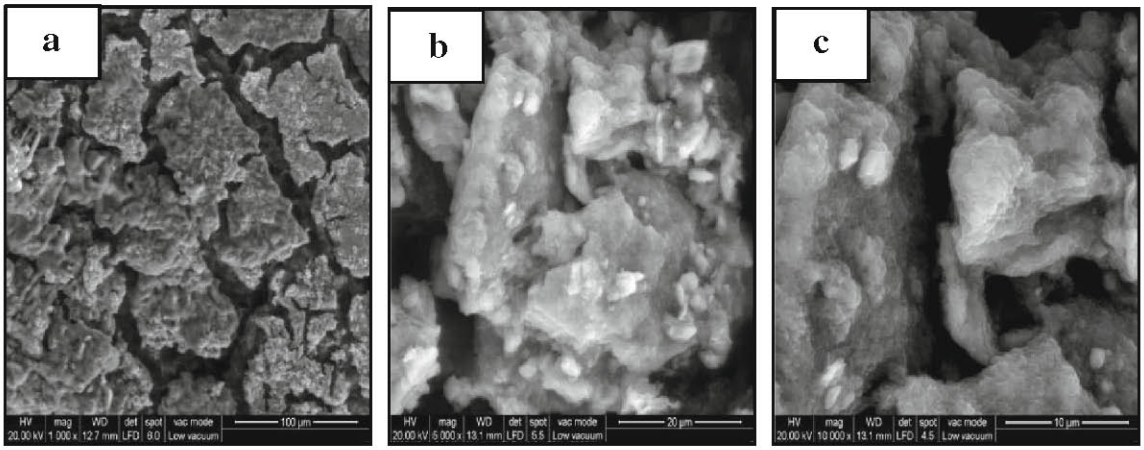

Fig. 3 SEM images of Ni-com electrode **a** 1000X, **b** 5000X, and **c** 10,000X

voltammograms exhibit the CV peaks corresponding to a redox process, the anodic nickel hydroxide oxidation peak, and the cathodic oxyhydroxide reduction peak. The oxygen evolution reaction is a parasitic process that decreases charging efficiency in the energy storage capacity of the system.

The CV curve corresponding to E-Ni-com electrodes shows that, at potentials around 0.5 V, the nickel hydroxide oxidation process overlaps with the oxygen evolution reaction and that a wide cathodic peak is located around 0.28 V.

The peak potential values corresponding to the oxidation/reduction Ni $(OH)_2$/NiOOH process are very well resolved for E-MWCNTsNi-PS electrodes (at 0.500 and 0.385 V, respectively). However, for E-MWCNTsNi-PhM electrodes, the oxidation reaction is overlapped with the oxygen evolution process and the reduction peak potential is located at less positive potentials. It should be noted that the difference between the anodic and cathodic peak positions ($\Delta E_{a,c}$) relates to the reversible insertion/de-insertion of H^+ in the nickel hydroxide/oxyhydroxide and is an important parameter to estimate the electrochemical properties of electrodes. The insertion of hydrogen takes place during discharging, and the inverse process occurs during charging. The CV data shown in Figure 6 indicates that E-MWCNTsNi-PS electrodes have a better reversibility and practically no overlap between the nickel hydroxide oxidation and oxygen evolution reactions.

The rate capability of the nickel electrode samples was investigated under six different current density rates, and the results are shown in Fig. 7. For both samples containing MWCNT (MWCNTsNi-PhM and MWCNTsNi-PS), it can be observed that for increasing discharge current values, the specific discharge capacity decreases slowly compared with those corresponding to Ni-com samples. These facts indicate that smaller overpotential values are involved in the electrochemical processes related to E-MWCNTsNi-PhM and MWCNTsNi-PS samples.

The Nyquist impedance spectra of E-MWCNTsNi-PhM and E-MWCNTsNi-PS electrodes at 50% SOD are shown in Fig. 8a. At high frequencies, the plots exhibit a linear behavior with a slope of approximately 45° related to the porous nature of the active material. The semicircle at the intermediate frequency range is associated with the combined effect of the charge-transfer resistance and double-layer capacitance. A Warburg-type impedance due to the proton diffusion processes appears at the low-frequency domain. The Bode representation of results in Fig. 8b shows that the impedance modulus

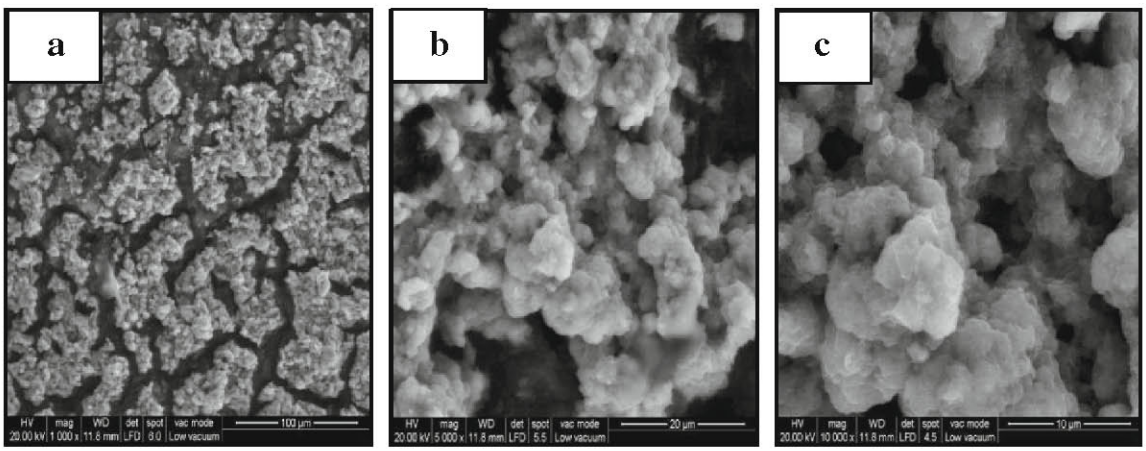

Fig. 4 SEM images of MWCNTsNi-PhM electrode **a** 1000X, **b** 5000X, and **c** 10,000X

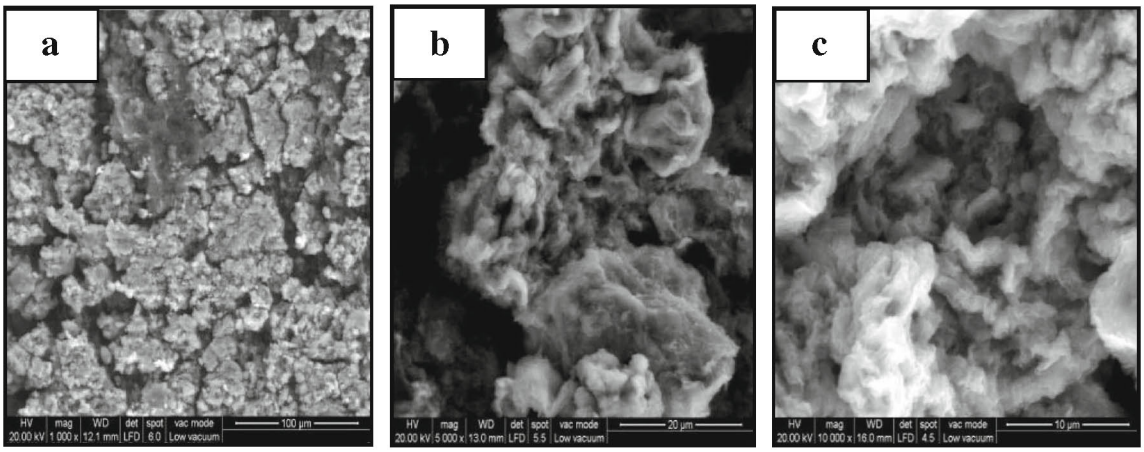

Fig. 5 SEM images of MWCNTsNi-PS electrode **a** 1000X, **b** 5000X, and **c** 10,000X

(|*Z*|) of E-Ni-com and E-MWCNTsNi-PhM electrodes are higher than those corresponding to E-MWCNTsNi-PS electrodes.

The EIS experimental results of Fig. 8 were fitted taking into consideration a physicochemical model proposed and described in previous publications that was developed based on the Nelder-Meade simplex search algorithm included in the MATLAB package [29–31]. The minimized objective function during the fitting procedure was the cost function J_p [31]. The fitting was considered acceptable when $J_p < 5 \times 10^{-3}$. The model takes into consideration that working electrode structures are porous and flooded by a highly concentrated electrolyte; the active material, pasted on the conducting support, is assumed to be composed of spherical NiOOH particles. Furthermore, the model considers that the charge transfer reaction taking place at the active material/electrolyte interface is coupled with proton transport in the active material.

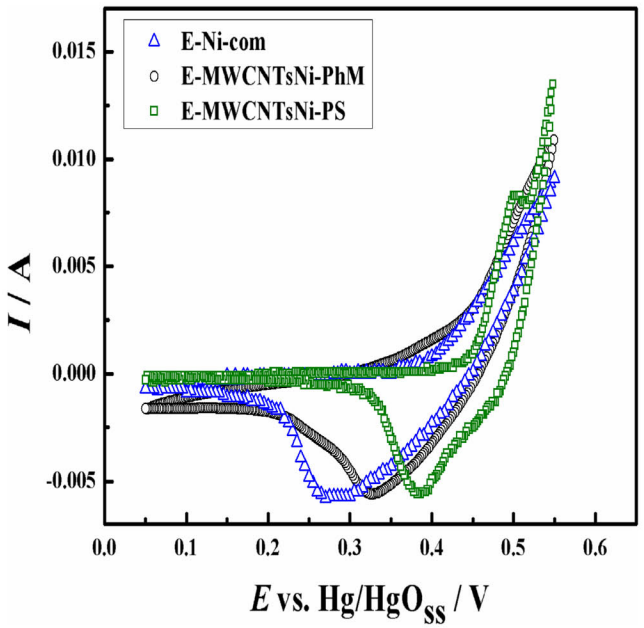

Fig. 6 Cyclic voltammetric curves of working electrodes

Consequently, the theoretical impedance of the system is described by the impedance of the porous electrode per unit geometric area (Z_p) as

$$Z_p(j\omega) = \frac{L}{A_p(\kappa+\sigma)}\left[1 + \frac{2 + \left(\frac{\sigma}{\kappa} + \frac{\kappa}{\sigma}\right)\cosh\nu(j\omega)}{\nu(j\omega)\sinh\nu(j\omega)}\right]$$

where

$$\nu(j\omega) = L\left(\frac{\kappa+\sigma}{\kappa\sigma}\right)^{1/2} Z_i^{-1/2}(j\omega)$$

L being the electrode thickness, A_p the electrode geometric area (cross section), and κ and σ the effective conductivities of the liquid and solid phases, respectively. The Z_i impedance of the solid/liquid interface per electrode unit volume (Ω cm^3) is derived considering the double-layer capacitance impedance (Z_{dl}) linked in parallel with the faradaic reaction impedance (Z_F).

$$Z_i^{-1} = Z_{dl}^{-1} + Z_F^{-1}$$

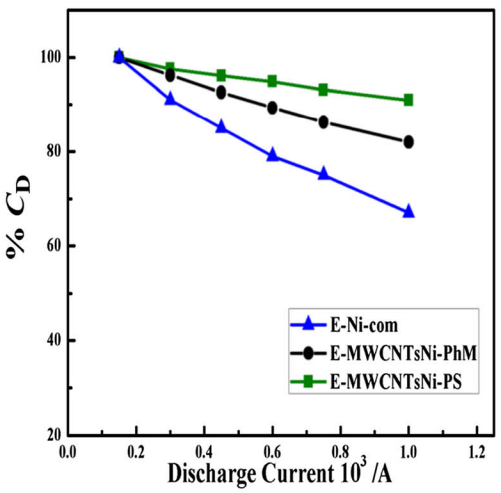

Fig. 7 Percent capacity of discharge (C_D) vs discharge currents of studied systems

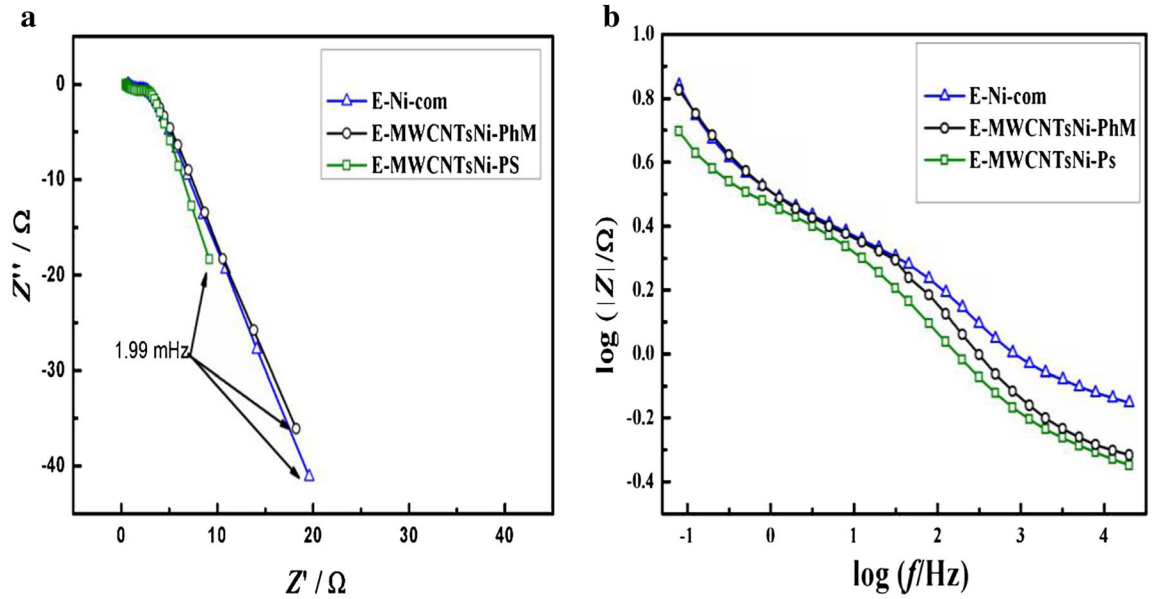

Fig. 8 Experimental EIS data of **a** Nyquist diagrams and **b** Bode plots

where

$$Z_{\mathrm{dl}} = \frac{1}{j\omega C_{\mathrm{dl}} a_e}$$

$j = \sqrt{-1}$; C_{dl} being the double-layer capacitance per unit interfacial area, a_e the interfacial area per unit volume (cm^{-1}), and $\omega = 2\pi f$ (f is the frequency of the perturbing signal, in Hz).

According to the previously described physicochemical model [29–31], Z_F is represented as

$$Z_F(\mathrm{j}\omega) = \frac{\mathrm{RT}}{i_0 F a_a} + \frac{\mathrm{RT}}{F^2 \mathrm{SOD}(1-\mathrm{SOD}) c_m a_a \sqrt{D}\sqrt{j\omega}}$$

where a_a is the active area per unit volume (cm^{-1}), SOD accounts for the state of discharge of the electrode, c_m corresponds to the maximum admitted proton concentration, i_0 is the exchange current density, and D is the proton diffusion coefficient.

The experimental EIS data (Fig. 8) were fitted according to the above described theoretical impedance function (Z_p). The fitting procedure allows identifying the physicochemical parameters related to the studied systems. Figure 9 shows the good agreement obtained between the measured and the fitted EIS data.

Table 1 lists the estimated structural and kinetic parameters of the studied electrodes obtained by fitting the experimental impedance data according to the above theoretical Z_p function. Table 1 shows that for the fixed value of 50% SOD, the E-MWCNTsNi-PS electrodes present higher values of C_{dl}, κ, and σ than those estimated for E-MWCNTsNi-PhM and E-Ni-com electrodes. These results could be explained taking into consideration that less compact and more porous systems (porosity factor is contained in the κ value [31]) are formed with E-MWCNTsNi-PS electrodes. These facts are in good agreement with SEM results (Fig. 5).

Furthermore, the studied systems present similar estimated parameter values of i_o and D, these values being in good agreement with those reported in the literature [32, 33].

Consequently, from the results in Table 1, we can conclude that the better electrochemical performance shown by E-MWCNTsNi-PS materials could be mainly associated with the increase in the effective conductivity of the solid phase (σ) and the double-layer capacitance per unit volume (C_{dl}) values.

Taking into consideration these results, the electrochemical performance improvement shown by MWCNTsNi-PS samples could be understood, considering that a different MWCNT distribution in the active material could be obtained depending on the preparation method. Thus, the addition of MWCNTs to precursor solutions before hydrothermal synthesis causes a significant improvement of the solid phase effective conductivity (σ), probably because this procedure is able to improve the network structure organization of the additive in active materials.

The analysis of overall results allows us to conclude that the addition of MWCNTs to precursor solutions before the hydrothermal synthesis increases the material utilization, the specific discharge capacity, and also improves the reversibility of the redox process.

According to these results, it is considered that one of the main reasons contributing to the high-discharge capacity values, obtained with MWCNT addition, is related to the decrease of the electrical resistance among the active material particles themselves and with the current collector that allow reducing the ohmic drop overpotential across the reaction interface.

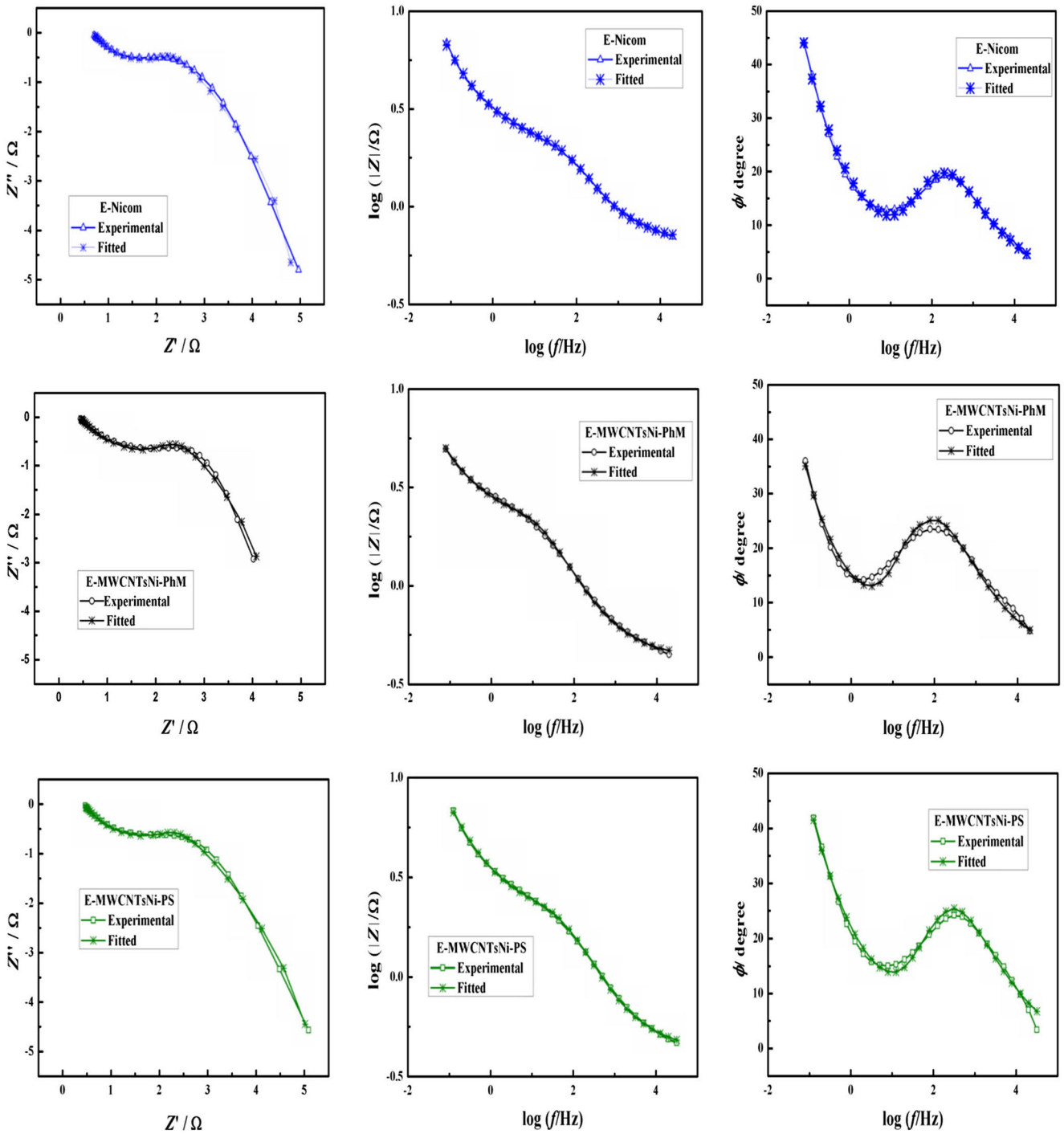

Fig. 9 Experimental and fitted EIS plots of systems

Table 1 Fitted parameters derived from EIS experimental data

Electrode	SOD	C_{dl} [F cm^{-3}] (±0.05)	κ [Ω^{-1} cm^{-1}] (±0.002)	σ [Ω^{-1} cm^{-1}] (±0.1)	i_o [A cm^{-2}] (±0.2 × 10^{-3})	D [cm^2 s^{-1}] (±0.3 × 10^{-12})
E-Ni-Com	50	0.081	0.032	0.72	1.13 × 10^{-3}	3.5 × 10^{-12}
E-MWCNTsNi-PhM		0.110	0.041	8.81	1.10 × 10^{-3}	5.8 × 10^{-12}
E-MWCNTsNi-PS		0.303	0.072	13.9	1.34 × 10^{-3}	8.1 × 10^{-12}

Conclusions

The β-Ni $(OH)_2$ active material was prepared by hydrothermal synthesis. The multiwall carbon nanotubes/nickel hydroxide composites (MWCNTs/Ni $(OH)_2$) were obtained by adding MWCNTs by two simple routes, before or after hydroxide preparation, incorporated in the precursor solutions or by physical mixing with the synthesized hydroxide, respectively. These materials were characterized by X-ray diffraction and transmission electron microscopy. They were used as active materials to prepare positive electrodes, and their electrochemical performance was studied and compared.

The physicochemical and structural parameters were estimated by fitting the EIS results according to a physicomathematical model. The E-MWCNTsNi-PS electrodes present higher effective conductivity of the solid phase (σ) and double-layer capacitance values (C_{dl}) than MWCNTsNi-PhM electrodes. It can be concluded that the addition of MWCNTs to precursor solutions before hydrothermal synthesis is more effective, from the conductivity (σ) improvement point of view, than MWCNT incorporation after synthesis of β-Ni $(OH)_2$ and consequently allow preparing cathode active materials for rechargeable alkaline nickel batteries. These facts can be understood considering that the first synthesis route is able to improve the network structure organization of the additive in active materials by favoring the electrical contact among the hydroxide particles.

Acknowledgments The authors gratefully acknowledge the financial support provided by the Agencia Nacional de Promoción Científica y Tecnológica (ANPCyT), Consejo Nacional de Investigaciones Científicas y Técnicas (CONICET), and Universidad Tecnológica Nacional (UTN).

References

1. Constantin DM, Rus EM, Oniciu L, Ghergari L (1998) The influence of some additives on the electrochemical behaviour of sintered nickel electrodes in alkaline electrolyte. J Power Sources 74:188–197
2. Yuan A, Cheng S, Zhang J, Cao C (1998) The influence of calcium compounds on the behaviour of the nickel electrode. J Power Sources 76:36–40
3. Li Y, Li W, Chou S, Chen J (2008) Synthesis, characterization and electrochemical properties of aluminum-substituted alpha-Ni $(OH)_2$ hollow spheres. J Alloys Compd 456:339–343
4. Dai J, Sam Li FY, Danny Xiao T, Wang DM, Reisner DE (2000) Structural stability of aluminum stabilized alpha nickel hydroxide as a positive electrode material for alkaline secondary batteries. J Power Sources 89:40–45
5. Cheng S, Anbao Y, Hong L, Jianqing Z, Chunan C (1998) Effects of barium and cobalt on electrochemical performance of nickel hydroxide with chemically co-precipitated zinc. J Power Sources 76:215–217
6. Yunchang D, Jiongliang Y, Hui L, Zhaorong C, Zcyun W (1995) A study of the performance of a paste-type nickel cathode. J Power Sources 56:201–204
7. Casas-Cabanas M, Hernandez JC, Gil V, Soria ML, Palacin MR (2004) On the key importance of homogeneity in the electrochemical performance of industrial positive active materials in nickel batteries. J Power Sources 134:298–307
8. Nathira Begum S, Muralidharan VS, Ahmed Basha C (2009) The influences of some additives on electrochemical behavior of nickel electrodes. Int J Hydrog Energy 34:1548–1555
9. Ortiz MG, Castro EB, Real SG (2014) Effect of cobalt electroless deposition on nickel hydroxide electrodes. Int J Hydrog Energy 39: 6006–6012
10. Liu X, Yu L (2004) Influence of nanosized Ni $(OH)_2$ addition on the electrochemical performance of nickel hydroxide electrode. J Power Sources 128:326–330
11. Treacy MMJ, Ebbesen TW, Gibson JM (1996) Exceptionally high Young's modulus observed for individual carbon nanotubes. Nature 381:678–680
12. Nardelli BM, Yakobson BI, Bernholc J (1998) Mechanism of strain release in carbon nanotubes. Phys Rev B 57(8):R4277–R4280
13. Wong EW, Sheehan PE (1997) Nanobeam mechanics: elasticity, strength, and toughness of nanorods and nonotubes. Science 277: 1971–1975
14. Chen JH, Li WZ, Wang DZ, Yang SX, Wen JG, Ren ZF (2002) Electrochemical characterization of carbon nanotubes as electrode in electrochemical double-layer capacitors. Carbon 40:1193–1197
15. Dai H, Wong EW, Lieber CM (1996) Probing electrical transport in nanomaterials: conductivity of individual carbon nanotubes. Science 272:523–526
16. Ebbesen TW, Lezec HJ, Hiura H, Bennett JW, Ghaemi HF, Thio T (1996) Electrical conductivity of individual carbon nanotubes. Nature 382:54–56
17. Song QS, Aravindaraj GK, Sultana H, Chan SLI (2007) Performance improvement of pasted nickel electrodes with multiwall carbon nanotubes for rechargeable nickel batteries. Electrochim Acta 53:1890–1896
18. Frackowiak E, Béguin F (2002) Electrochemical storage of energy in carbon nanotubes and nanostructured carbons. Carbon 40:1775–1787
19. Niu C, Sichel EK, Hoch R, Moy D, Tennent H (1997) High power electrochemical capacitors based on carbon nanotube electrodes. Appl Phys Lett 70:1480–1482
20. Wang XF, Ruan DB, You Z (2006) Application of spherical Ni (OH)z/CNTs composite electrode in asymmetric supercapacitor. Trans Nonferrous Metals Soc China 16:1129–1134
21. Liu C-G, Lee Y-S, Kim Y-J, Song I-C, Kim J-H (2009) Electrochemical characteristics of hydrothermally deposited nickel hydroxide on multi-walled carbon nanotube for supercapacitor electrode. Synth Met 159:2009–2012
22. Schlapbach L, Zuttel A (2001) Hydrogen-storage materials for mobile applications. Nature 414:353–358
23. Prosini PP, Pozio A, Botti S, Ciardi R (2003) Electrochemical studies of hydrogen evolution, storage and oxidation on carbon nanotube electrodes. J. Power Sources 118:265–269
24. Scott MR, Dixon BG, Gennett T, Raffaelle R, Heben MJ (2004) High-energy, rechargeable Li-ion battery based on carbon nanotube technology. J. Power Sources 138:277–280
25. Frackowiak E, Gautier S, Gaucher H, Bonnamy S, Beguin F (1999) Electrochemical storage of lithium multiwalled carbon nanotubes. Carbon 37:61–69
26. Lv J, Tu JP, Zhang WK, Wu JB, Wu HM, Zhang B (2004) Effects of carbon nanotubes on the high-rate discharge properties of nickel/metal hydride batteries. J. Power Sources 132:282–287

27. Real SG, Ortiz MG, Castro EB (2017) Electrochemical characterization of nickel hydroxide nanomaterials as electrodes for Ni-MH batteries. J Solid State Electrochem 21(1):233–241
28. Ortiz MG, Castro EB, Real SG (2016) Electrochemical characterization of MWCNTs/Ni (OH)2 composites as cathode materials. J Solid State Electrochem 20(4):1029–1036
29. De Levie R (1967) In: Delahay P (ed) Advances in electrochemistry and electrochemistry engineering, 6. Interscience, NY, pp 329–361
30. Castro EB, Cuscueta DJ, Milocco RH, Ghilarducci AA, Salva HR (2010) An EIS based study of a Ni-MH battery prototype. Modeling and identification analysis. Int J Hydrog Energy 35: 5991–5998
31. Ortiz MG, Becker D, Garaventta G, Visintin A, Castro EB, Real SG (2011) Dynamic monitoring of structural changes in nickel hydroxide electrodes during discharge in batteries. Electrochim Acta 56(23):7946–7954
32. Paxton B, Newman J (1997) Modeling of nickel/metal hydride batteries. J Solid State Electrochem 144(11):3818–3831
33. Mao Z, De Vidts R, White RE, Newman J (1994) Theoretical analysis of the discharge performance of a NiOOH/H2 cell. J Electrochem Society 141:54–64